1999-01-01

Micropolarizer Array for Infrared Imaging Polarimetry

M. W. Jones

Gregory P. Nordin
nordin@byu.edu

P. C. Deguzman

J. T. Meier

Original Publication Citation

G. P. Nordin, J. T. Meier, P. C. Deguzman, and M. W. Jones, "Micropolarizer Array for Infrared Imaging Polarimetry", J. Opt. Soc. Am. A 16(5), pp. 1184-1193 (1999)

Micropolarizer array for infrared imaging polarimetry

Gregory P. Nordin

Department of Electrical and Computer Engineering, University of Alabama in Huntsville, Huntsville, Alabama 35899

Jeffrey T. Meier

Nichols Research Corporation, Systems Development and Evaluation Center, P.O. Box 400002, Huntsville, Alabama 35815

Panfilo C. Deguzman

Department of Electrical and Computer Engineering, University of Alabama in Huntsville, Huntsville, Alabama 35899

Michael W. Jones

Nichols Research Corporation, Systems Development and Evaluation Center, P.O. Box 400002, Huntsville, Alabama 35815

Received August 14, 1998; revised manuscript received January 21, 1999; accepted January 22, 1999

The design and fabrication of a micropolarizer array for imaging polarimetry is described for the 3–5-μm-wavelength region. Each micropolarizer consists of a 475-nm-period Mo wire grid in a 16 μm $\times$ 16 μm aperture. Interference lithography is used to generate the small grating features through an etch mask layer. Arrays of 256 $\times$ 256 micropolarizers at three distinct angular orientations have been fabricated that permit the measurement of the first three Stokes vector components in each pixel of an imaging polarimeter. An imaging system composed of a micropolarizer array integrated directly onto a focal plane array has been assembled, and initial testing has been performed. © 1999 Optical Society of America [S0740-3232(99)01905-5]

OCIS codes: 230.5440, 050.1970, 220.4610, 050.1950, 110.3080, 260.5430.

1. INTRODUCTION

Infrared (IR) imaging systems have found application in a wide variety of areas. Currently, imaging polarimetry is being investigated to extend the capabilities of IR systems beyond conventional amplitude imaging.[1,2] For example, some polarization metrics used in imaging polarimetry offer the capability to highlight or suppress different materials in a scene or objects at different orientations. Hence imaging polarimetry offers a path to extending the capabilities of conventional IR imaging and to providing new imaging modalities.

Available polarization metrics include measurement of the full polarization properties of the imaged light (i.e., all four components of the Stokes vector for each image pixel) or some subset of those properties (such as the first two or three Stokes vector components). Measuring any or all of the polarization components typically involves manipulating a temporal sequence of images, each of which is acquired by means of looking through either a rotated polarization filter or a sequence of different polarization filters. This time-sequential approach limits the utility of such imaging systems to situations in which both the scene and the camera are stationary.

In this paper we describe the design and fabrication of a micro-optical element composed of an array of small-aperture polarizers (i.e., micropolarizers) that can be integrated directly onto the focal plane array (FPA) of an IR imaging system. This element allows the simultaneous determination of the first three Stokes vector components within a single image frame, hence permitting the realization of real-time (video frame rate) imaging polarimetry. Each micropolarizer consists of a wire grid at one of three angular orientations and is designed to operate in the 3–5-μm-wavelength region. Although the fabrication of iodide-doped polyvinyl alcohol-based micropolarizer arrays has recently been reported for use in the visible-wavelength region,[3] to our knowledge the work discussed in this paper represents the first physical realization of an array of wire grid micropolarizers.

The design of the micropolarizer array and of the individual micropolarizers is discussed in Section 2. In Section 3 we review the fabrication method used to create a three-state micropolarizer array. Experimental results and initial imagery from an integrated camera system are presented in Section 4.

2. DESIGN

High-spatial-frequency metal gratings have long been recognized as an effective polarizer option for the IR portion of the spectrum.[4,5] We therefore elected to fabricate the micropolarizer array by patterning small-aperture

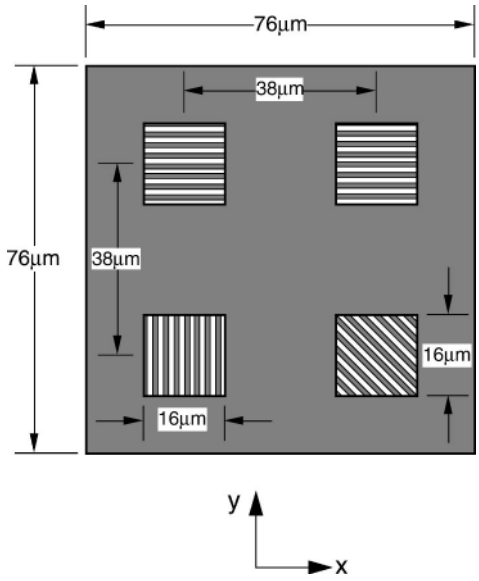

Fig. 1. Schematic diagram of unit cell containing a 2 × 2 array of micropolarizers.

wire grids in a thin metallic film deposited on a silicon substrate. Molybdenum was chosen for the metal layer because of its excellent reflection properties in the mid-IR and the relative ease with which it can be patterned by reactive ion etching.

The micropolarizer array consists of a 128 × 128 array of unit cells, each of which is composed of a 2 × 2 array of micropolarizers. As illustrated in Fig. 1, each unit cell is 76 μm on a side. The micropolarizers are located on 38-μm centers with 16 μm × 16 μm apertures. The top two micropolarizers pass illumination linearly polarized along the y axis, while the bottom left-hand and the bottom right-hand micropolarizers pass linearly polarized light oriented along the x axis and at 45° counterclockwise to the x axis, respectively.

A fabricated micropolarizer array is integrated directly onto a 256 × 256 pixel FPA such that the micropolarizer side of the Si substrate is immediately adjacent to the FPA front surface, with each micropolarizer spatially aligned to a corresponding FPA pixel (which are 38 μm square). Each unit cell of 2 × 2 micropolarizers and concomitant 2 × 2 FPA pixels is considered to comprise a single pixel in the image generated by the integrated system (these will be termed image pixels to differentiate them from FPA pixels). The system therefore produces images of 128 × 128 image pixels.

The first three Stokes vector components, S_0, S_1, and S_2, are calculated for each of these image pixels according to[6,7]

$$S_0 = I_0 + I_{90},$$
$$S_1 = 2I_0 - S_0,$$
$$S_2 = 2I_{45} - S_0, \quad (1)$$

in which I_0, I_{45}, and I_{90} are the signals measured through the micropolarizers oriented at 0°, 45°, and 90° counterclockwise to the x axis, respectively. Note that in this particular imaging polarimeter implementation the measurements I_0, I_{45}, and I_{90} in each image pixel come from slightly displaced regions within the image pixel. This tends to affect the polarimetric measurement of object edges, leading in some cases to edge enhancement. Additional functionality to be incorporated in follow-on micro-optical elements will lead to the co-registration of an image across the different micropolarizer orientations. Also note that only one polarizer, designed to pass 90° linearly polarized light, is needed to calculate the Stokes vector components in Eqs. (1). The second polarizer of this orientation will be used in a later micro-optical implementation as part of measuring S_3.

Rigorous coupled-wave analysis[8,9] was used to design the polarizers to achieve an extinction ratio of greater than or equal to approximately 20 over the 3–5-μm-wavelength region. We define extinction ratio as T_{TM}/T_{TE}, in which T_{TM} and T_{TE} are the power transmission coefficients for TM (electric-field vector perpendicular to the wire grid fingers) and TE (electric-field vector parallel to the wire grid fingers) polarized light, respectively. For the simulation results discussed below, normally incident plane-wave illumination is assumed, and the period of the wire grid is taken to be 475 nm. The cross section of each wire is assumed to be rectangular.

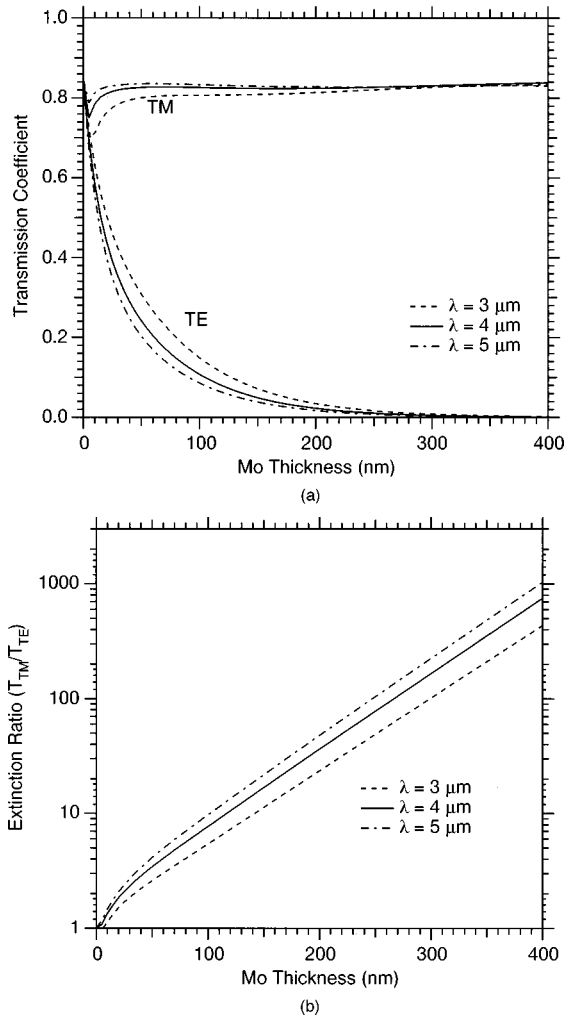

Fig. 2. Simulation results for (a) TE and TM transmitted power and (b) extinction ratio as a function of metal thickness for a Mo wire grid polarizer on Si (normal-incidence illumination, 475-nm grating period, 30% Mo fill factor).

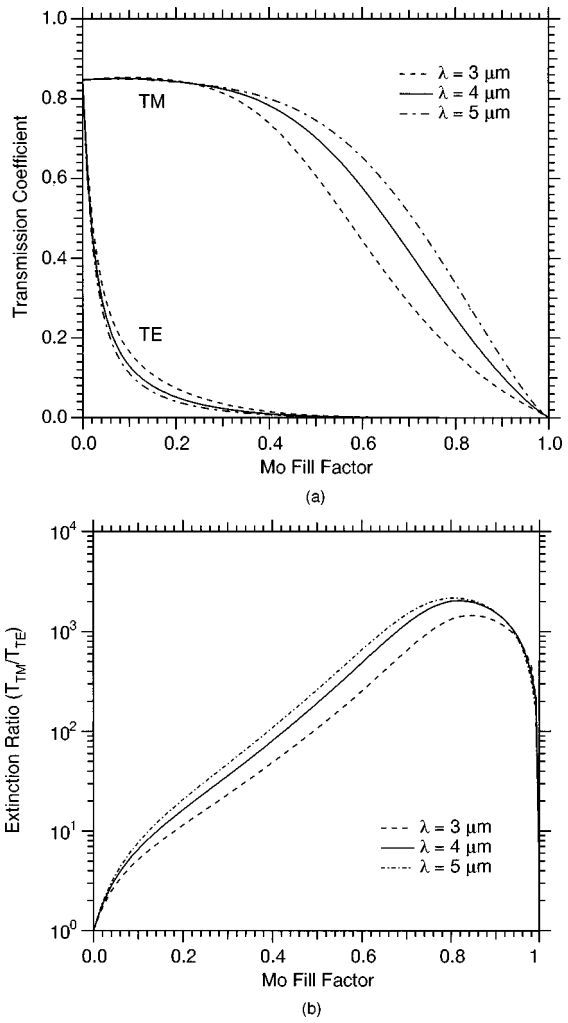

Fig. 3. Simulation results for (a) TE and TM transmitted power and (b) extinction ratio as a function of metal fill factor for a Mo wire grid polarizer on Si (normal-incidence illumination, 475-nm grating period, 200-nm Mo thickness).

The incident material is Si, and the wire grid grooves and exit medium are assumed to have a refractive index of 1.5 (corresponding to a glue layer between the micropolarizer and the FPA's). The optical constants of the as-deposited Mo films were determined by Surface Optics of San Diego, California based on hemispherical directional reflectance measurements.[10] In the 3–5-μm-wavelength range the real, n, and the imaginary, k, components of the refractive index are well approximated by simple quadratic expressions:

$$n = -1.715 + 2.957\lambda - 0.1060\lambda^2,$$
$$k = 0.3483 + 4.366\lambda - 0.2528\lambda^2. \quad (2)$$

Figures 2(a) and 2(b) show the transmission coefficients and resultant extinction ratio, respectively, as a function of the Mo wire grid thickness for a fill factor of 30% (fill factor is defined here as the ratio of the width of a single Mo wire to the wire grid period). The TE transmission coefficient decreases rapidly with increasing Mo thickness, while the TM coefficient is approximately the same as what is predicted for Fresnel transmission in the absence of the wire grid. As can be seen in Fig. 2(b), the extinction ratio is greater than 20 over the 3–5-μm-wavelength region for a Mo thickness of 200 nm.

Our fabrication experience indicates that the Mo wire grid fill factor can be difficult to precisely control. It is therefore important to understand how the extinction ratio depends on the fill factor. Figure 3 shows the transmission coefficients and the extinction ratio, respectively, for a 200-nm-thick wire grid as a function of the Mo fill factor. The TE transmission coefficient decreases rapidly as the fill factor increases, while the TM transmission coefficient stays relatively constant for small fill factors (up to ~0.4) and then drops significantly with increasing fill factor. However, as can be seen in Fig. 3(b), the extinction ratio increases by nearly 3 orders of magnitude as the fill factor goes from 0.05 to 0.8, indicating that the TE transmission coefficient decreases more rapidly with increasing fill factor than does the TM transmission coefficient. The extinction ratio clearly is a sensitive function of the fill factor. Our target design requires a fill factor of approximately 0.3 or greater to achieve the desired extinction ratio.

3. MICRO-OPTICAL ELEMENT FABRICATION

Fabrication of the 475-nm-period wire grids is the most challenging aspect of physically implementing the designed micro-optical element. Interference lithography was selected as a straightforward means of generating the requisite small-period grating structures.[11–14] The basic recording setup is shown in Fig. 4. The optical source is a HeCd laser with emission at 442 nm.

The three different angularly oriented sets of micropolarizers are formed sequentially. The basic fabrication process for each polarizer orientation is illustrated in Fig. 5. The starting point [Fig. 5(a)] is a uniform SiO_2 masking layer deposited on a 200-nm Mo film (which is on a 75-mm Si wafer). Both layers are deposited by RF sputtering. Apertures are then opened in the SiO_2 film that reveal the Mo to be patterned during the current fabrication iteration. This is illustrated in Fig. 5(b) for a single aperture. Next, a bottom-layer antireflection coating (ARC) is applied, followed by photoresist. The ARC layer is necessary to avoid standing waves in the photoresist, which is 500 nm thick. After the photoresist is exposed in the interference exposure setup and is developed,

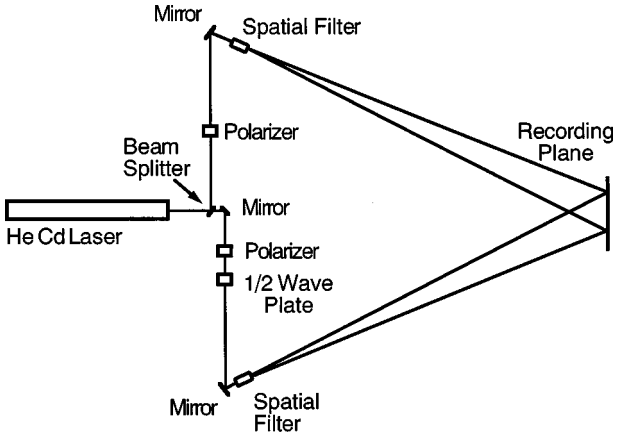

Fig. 4. Schematic diagram of interferometric exposure setup.

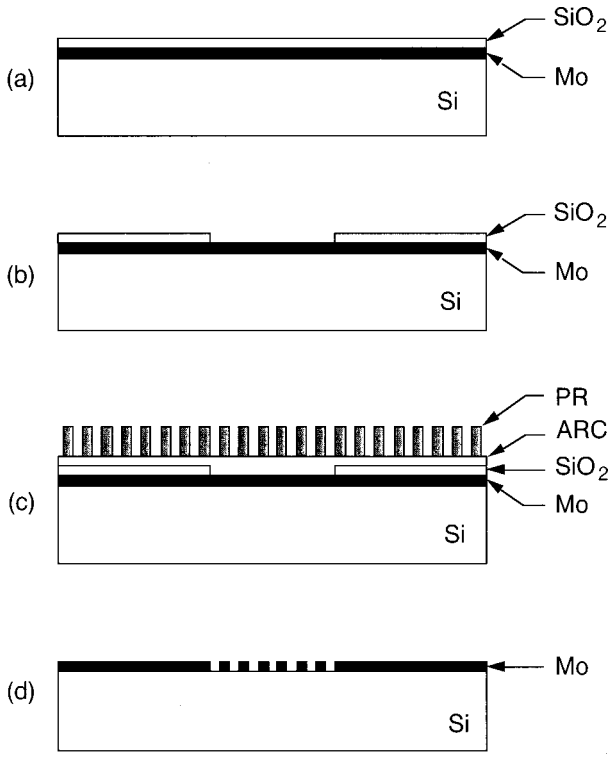

Fig. 5. Schematic illustration of micropolarizer fabrication steps for a single angular orientation: (a) SiO_2 masking layer deposited on Mo, (b) windows patterned in SiO_2, (c) result of interference lithography, (d) after metal etch and strip of other layers.

the photoresist pattern is transferred into the ARC. The Mo is then reactive ion etched with a fluorine-based etch chemistry to form the Mo grating. A two-stage Mo etch is used to minimize undercutting of the underlying Si. After stripping of the photoresist, ARC, and SiO_2, a new SiO_2 layer is deposited, and this same sequence of steps is used to form the next set of micropolarizers.

4. RESULTS

By means of the above procedure, numerous wire grid micropolarizer arrays have been fabricated. Typical results are shown in Figs. 6 and 7. Top-view scanning electron microscope (SEM) images for each micropolarizer angular orientation are shown in Fig. 6. Note the excellent wire grid definition and uniformity within the apertures, as well as the sharp aperture edges. Figure 7(a) shows a SEM cross-sectional view of an entire 90° micropolarizer. Close-up views of the central portion and of the left-hand edge of the aperture are shown in Figs. 7(b) and 7(c), respectively. The Mo grating fill factor for this particular micropolarizer is approximately 25%, and the sidewall angles are ~84°. Undercutting of the Si substrate has clearly been avoided, although the Si visible in the grating troughs has been roughened by the Mo etch. After fabrication of the Mo wire grids, final devices are coated with a 280-nm SiO_2 protective layer. A SEM cross-sectional view of the left-hand edge of a coated micropolarizer with a fill factor of ~30% is shown in Fig. 8.

We do not yet have the capability of directly measuring the extinction ratio of a single micropolarizer. However, we have measured the extinction ratio of similar large-aperture (~1-cm) wire grid polarizers fabricated by the same process described in Section 3, except without the SiO_2 masking layer. For example, a 134-nm-thick wire grid polarizer with a 41% Mo fill factor yields a measured extinction ratio of 13. This result compares well with a

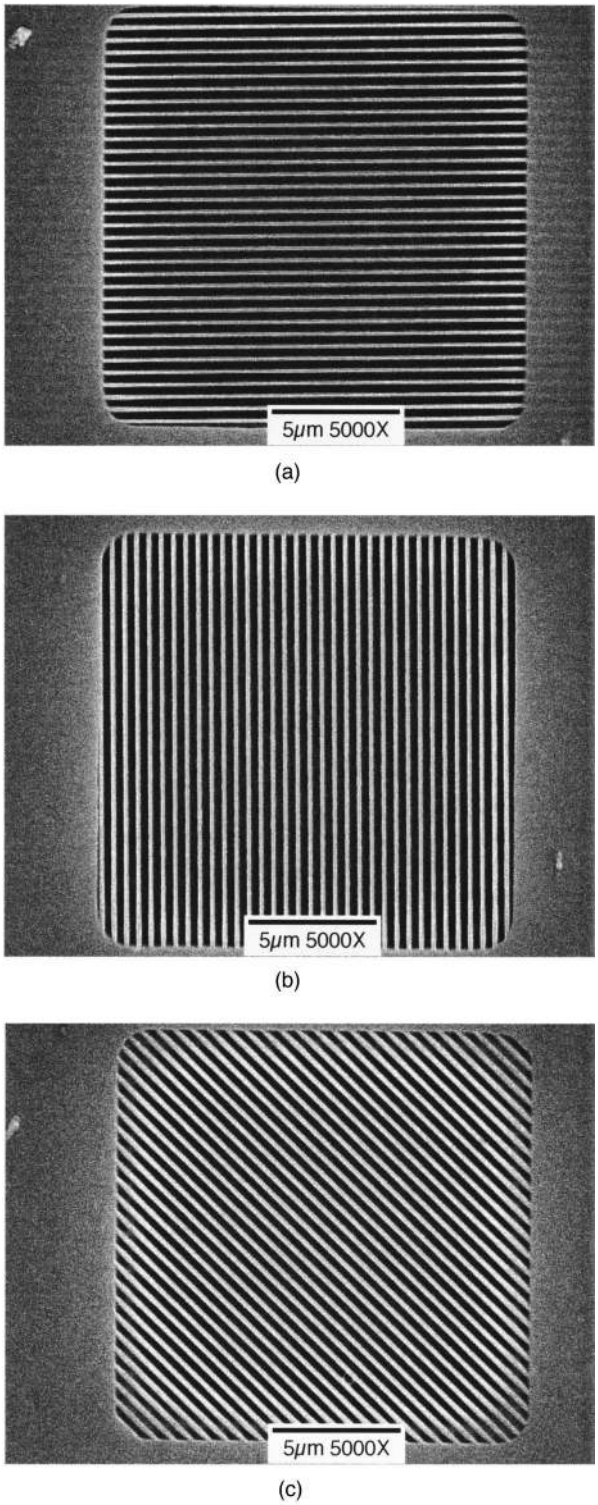

Fig. 6. Top-view SEM images of wire grid polarizers that pass (a) vertical, (b) horizontal, and (c) 45° linearly polarized light.

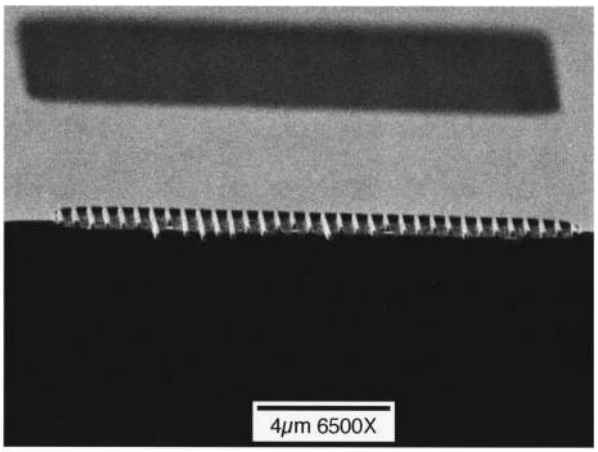

(a)

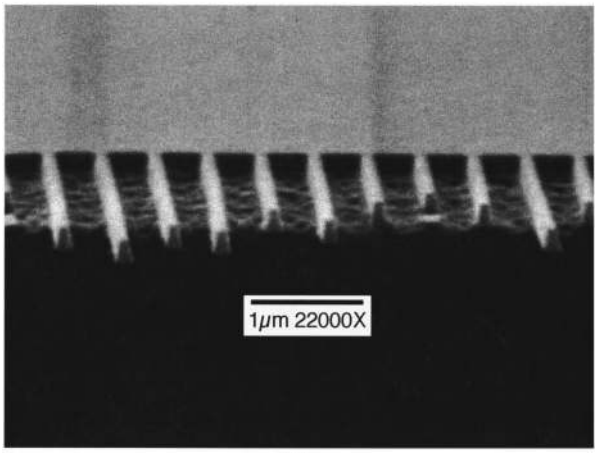

(b)

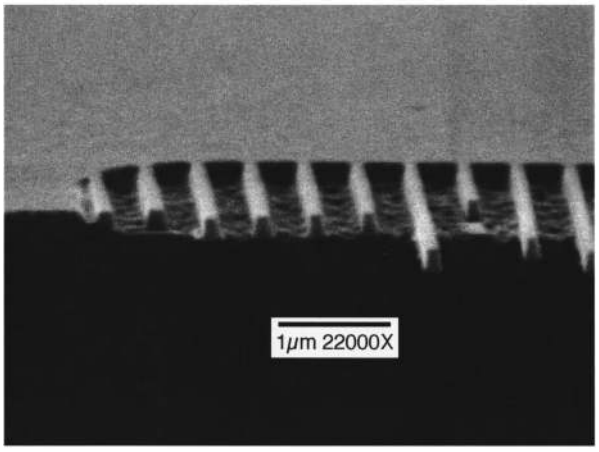

(c)

Fig. 7. SEM cross-sectional images of (a) 16-μm-wide 90° polarizer, (b) close-up view of the center of (a), and (c) close-up view of the left-hand side of (a).

predicted extinction ratio of 14 for the same wire grid polarizer geometry. We do find, however, that there is some discrepancy between measured and predicted extinction ratios for low-fill-factor wire grid polarizers, with the measured values being a factor of ~3 smaller than predictions when the fill factor is between 25% and 35%. Since the fill factor of the micropolarizers in our polarizer arrays falls within this range, the micropolarizers likely have a lower extinction ratio than their design calls for. We are currently investigating the reason for this difference. In the meantime, we have recently developed an alternative wire grid polarizer fabrication process with which we have created large-aperture (~1-cm) polarizers with measured extinction ratios of approximately 200. In this fabrication process a thin chromium layer is deposited after the ARC is patterned. The ARC and the photoresist are then removed to effect lift-off of the Cr. The resultant Cr lines are then used as an etch mask for the Mo etch. The advantage of this process is that Mo fill factors of 50% or more are readily achievable, which in turn results in larger extinction ratios. We expect to soon fabricate arrays of high-extinction-ratio micropolarizers by this alternative process.

A micropolarizer array fabricated as described in Section 3 has been integrated with a FPA into an IR camera system. A sample of the initial imagery is shown in Fig. 9. For this image the signal level in each pixel is S_1 normalized by S_0. Although the micropolarizer extinction ratio is likely small, the polarization signature of the ve-

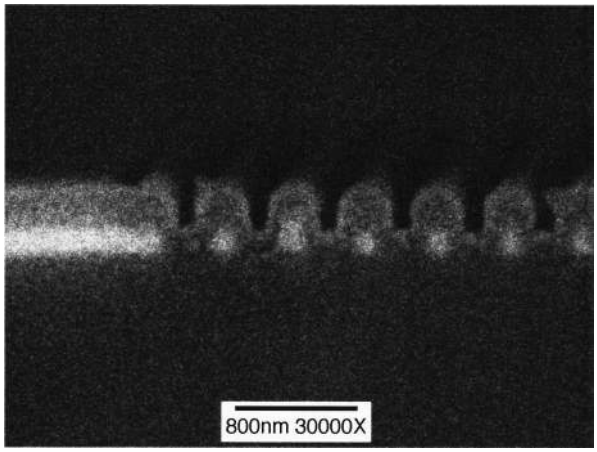

Fig. 8. SEM image of grating cross section with SiO_2 capping layer.

Fig. 9. Sample of initial imagery obtained with integrated micropolarizer and FPA camera system.

(a)

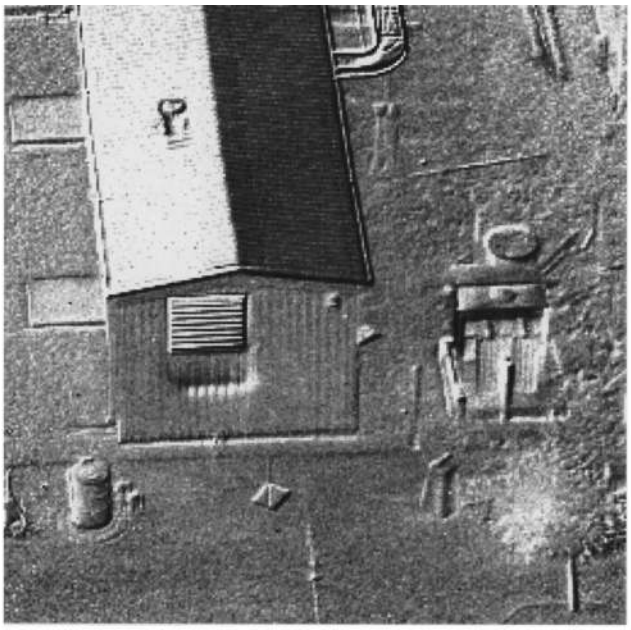

(c)

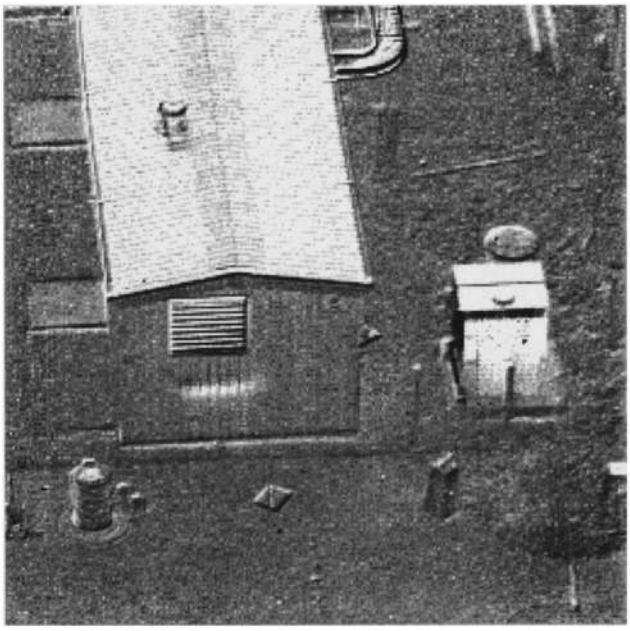

(b)

Fig. 10. (a)–(c) Images of a static scene for the S_0, S_1, and S_2 Stokes vector components, respectively.

hicle differentiates it relative to the background. Also, there appears to be some enhancement of the vehicle edges.

As a simple example of the potential of imaging polarimetry, consider the sequence of images shown in Fig. 10. These were taken with a camera system employing a time-sequential variation of polarization filters to obtain polarization information from a stationary scene, which was observed at night. The S_0 Stokes vector component is shown in Fig. 10(a), which is equivalent to a typical IR image. Figure 10(b) shows the same scene, except each pixel value consists of the S_1 Stokes vector component (i.e., the amount of horizontal linear polarization for each pixel). Note that, compared with the S_0 image, more detail is apparent in the small shed to the right of the building, as well as in several other small features in the scene. This enhanced contrast is dependent on the material properties and orientation of the objects relative to the camera. An example of this is illustrated in Fig. 10(c), which consists of the S_2 Stokes vector component. In this case there is contrast between the left-hand and the right-hand halves of the building's roof because they are at different angular orientations relative to the 45° linear polarizer filter of the camera. This is not apparent in Fig. 10(b) because the angular orientation of the two halves of the roof are symmetric about the horizontal pass

axis of the polarization filter. Hence polarization information can be used to highlight different aspects of a scene.

5. SUMMARY

In this paper we have described the design and fabrication of an array of 256 × 256 micropolarizers at three different angular orientations for application in IR imaging polarimetry. Each micropolarizer consists of a wire grid fabricated in a Mo film on a Si substrate. SEM evaluation indicates successful fabrication of the desired structures. Initial results from an IR imaging system composed of an integrated micropolarizer and focal plane array that measures the first three Stokes vector components have been presented. Despite likely low micropolarizer extinction ratios, polarization information in observed scenes has been obtained.

Our future research will include integration of higher-extinction-ratio wire grid structures into micropolarizer arrays, development of micro-optical elements that measure all four Stokes vector components, co-registration of the image at each polarization-sensing element in a 2 × 2 array, and scale-up to larger numbers of pixels.

REFERENCES

1. T. J. Rogne, F. G. Smith, and J. E. Rice, "Passive target detection using polarized component of infrared signatures," in *Polarimetry: Radar, Infrared, Visible, Ultraviolet, and X-Ray*, R. A. Chipman and J. W. Morris, eds., Proc. SPIE **1317**, 242–251 (1990).
2. C. S. L. Chun, D. L. Fleming, and E. J. Torok, "Polarization-sensitive thermal imaging," in *Automatic Object Recognition IV*, F. A. Sadjadi, ed., Proc. SPIE **2234**, 275–286 (1994).
3. E. J. Guo and D. J. Brady, "Fabrication of high-resolution micropolarizer arrays," Opt. Eng. **36**, 2268–2271 (1997).
4. G. R. Bird and M. Parrish, Jr., "The wire grid as a near-infrared polarizer," J. Opt. Soc. Am. **50**, 886–891 (1960).
5. B. J. B. Young, H. A. Graham, and E. W. Peterson, "Wire grid infrared polarizer," Appl. Opt. **4**, 1023–1026 (1965).
6. M. Born and E. Wolf, *Principles of Optics*, 6th ed. (Pergamon, New York, 1986), p. 554.
7. E. Hecht, *Optics*, 3rd ed. (Addison-Wesley, Reading, Mass., 1998), p. 366.
8. M. G. Moharam, E. B. Grann, D. A. Pommet, and T. K. Gaylord, "Stable implementation of the rigorous coupled-wave analysis for surface-relief gratings: enhanced transmittance matrix approach," J. Opt. Soc. Am. A **12**, 1077–1086 (1995).
9. L. Li, "Use of Fourier series in the analysis of discontinuous periodic structures," J. Opt. Soc. Am. A **13**, 1870–1876 (1996).
10. R. J. Champetier and G. J. Friese, "Use of polished fused silica to standardize directional polarized emittance and reflectance measurements in the infrared," SAMSO Rep. TR-74-202 from the Aerospace Corporation to the Space and Missile Systems Organization (Space and Missile Systems Organization, Air Force Systems Command, Los Angeles, Calif., 1974).
11. L. Mashev and S. Tonchev, "Formation of holographic diffraction gratings in photoresist," Appl. Phys. A **26**, 143–149 (1981).
12. K. Yokomori, "Dielectric surface-relief gratings with high diffraction efficiency," Appl. Opt. **23**, 2303–2310 (1984).
13. R. D. Boyd, J. A. Britten, D. E. Decker, B. W. Shore, B. C. Stuart, M. D. Perry, and L. Li, "High-efficiency metallic diffraction gratings for laser applications," Appl. Opt. **34**, 1697–1706 (1995).
14. H. T. Nguyen, B. W. Shore, S. J. Bryan, J. A. Britten, R. D. Boyd, and M. D. Perry, "High-efficiency fused-silica transmission gratings," Opt. Lett. **22**, 142–144 (1997).